npj | clean water

www.nature.com/npjcleanwater

ARTICLE OPEN

Check for updates

Tunable nanostructured stainless-steel coating for high-selective and high-permeable separation membranes for oil/water emulsions

Yi-Jui Yeh[1], Jinn P. Chu[2]✉, Jhen-De You[3], Ting-Hao Chang[2], Jr Rong Liou[1], Wei-Hung Chiang[4], Pakman Yiu[5], Chun-Hway Hsueh[3], Yu-Lin Shen[6] and Kuo-Lun Tung[1,7]✉

This paper demonstrates a stainless-steel (SS) nano-pyramid structure (diameter of ~20–50 nm and pore size of 156.1 nm) sputter-coated on mixed cellulose ester (MCE) membrane for the use in separation of oil/water emulsions. SS-coated MCE membrane presented a superhydrophilic, antifouling surface as well as underwater superoleophobicity. The coated membrane achieved excellent separation efficiency of >99% when applied to light oil-water emulsions with a range of viscosities and densities. The highest permeation flux measured was 1,555 L m^{-2} h^{-1} when applied to toluene-in-water emulsions. The membrane also presented outstanding recyclability, as evidenced by oil rejection rate retaining at >99% through four separation cycles. The coated membrane was also shown to work well under harsh conditions including salty water, extreme pH values (1–14), and high temperatures (60 °C). In addition, our fabrication route of SS-coated MCE employs low process temperature while being highly scalable, which is favorable for industrial-scale applications.

npj Clean Water (2023)6:17 ; https://doi.org/10.1038/s41545-023-00237-x

INTRODUCTION

Oil pollution is an important concern in the petro-chemical industry[1,2], semiconductor manufacturing[1,3], and food industries[4,5]. There is a pressing need for cost-effective and energy-efficient technology by which to treat oily wastewater. The methods used to treat wastewater depend largely on the size of the oil droplets, which can be classified as follows: emulsified oil (droplet size of <20 μm), dispersed oil (droplet size of 20–150 μm), and free oil (droplet size >150 μm). Among them separation of emulsified oil from water is particularly difficult, due to the size of the oil droplet, the stability of oil/water emulsions, and the low concentration of oil[6–8]. Industrial approaches to the separation of oil from water include gravity separation, skimming, and dissolved air flotation[9]. Researchers have also developed methods involving aerogels[10], magnetic materials[11,12], and fluorosurfactant polymers[13]. Nonetheless, none of these methods are effective in dealing with emulsified oils, particularly those with droplets smaller than one micron[14]. There is a pressing need for an efficient and cost-effective system for the treatment of oily wastewater at industrial scales.

Membrane-based systems have shown particular promise for the separation of micro- and nanosized oil particles from oil-in-water emulsions, due to low energy consumption and a compact ecological footprint[15,16]. Note, however, that the separation efficiency and long-term stability of these systems depends on the resistance of the membrane to oil-fouling and a high-throughput rinsing system. Recent developments in superhydrophilic-underwater superoleophobic membranes have attracted the interest of researchers, due primarily to their high affinity for water, which allows for high permeability and ultralow or even near-zero oil adhesion[17,18]. Researchers have identified a number of organic polymers with outstanding wettability and high oil/water selectivity ideally suited to commercial oil/water separation at commercial scales[19]. Nevertheless, most polymers are unable to tolerate high temperatures and suffer from low separation efficiency. Separating oil/water (O/W) emulsions generally involves synthetic membranes made of organic, inorganic or hybrid organic-inorganic materials[20–22]. Efforts to achieve high permeability (separation flux) with high selectivity (separation efficiency) have led to the development of nanomaterial membranes with superhydrophilic surfaces and superoleophobicity in water[8,20,23]. Unfortunately, most of these membranes impose a trade-off between permeability and selectivity.

Numerous surface modification methods have been used in the fabrication of materials for O/W emulsion separation, including hydrothermal treatment [$MnMoO_4$], sputtering [metallic glass], and chemical vapor deposition [TiO_2 nanoparticles]. Note that sputter deposition is well-suited to large-scale commercial production, and the fact that it can be performed at room temperature means that it can be used with organic membranes. In the current study, we deposited a thin nano-structural stainless-steel coating on the surface of the polymer membrane via sputtering (physical vapor deposition; PVD). Large-area polymer membranes could be fabricated via sputter deposition in conjunction with roll-to-roll manufacturing systems.

In a previous study[24], we used sputter deposition to fabricate a stainless-steel (SS) coating with nano-scale pyramidal surface structures on silicon, which provided excellent hydrophilicity (water contact angle of 11°). The SS coatings also demonstrated

[1]Department of Chemical Engineering, National Taiwan University, Taipei 106216, Taiwan. [2]Department of Materials Science and Engineering, National Taiwan University of Science and Technology, Taipei 106335, Taiwan. [3]Department of Materials Science and Engineering, National Taiwan University, Taipei 106216, Taiwan. [4]Department of Chemical Engineering, National Taiwan University of Science and Technology, Taipei 106335, Taiwan. [5]Department of Materials Engineering, Ming Chi University of Technology, New Taipei City 243303, Taiwan. [6]Department of Mechanical Engineering, University of New Mexico, Albuquerque, NM 87131, USA. [7]Advanced Research Center for Green Materials Science and Technology, National Taiwan University, Taipei 106216, Taiwan. ✉email: jpchu@mail.ntust.edu.tw; kltung@ntu.edu.tw

good anti-fouling behavior, biological inertness, and durability in terms of strength, ductility, and corrosion resistance. In the current study, we applied this nano-pyramid SS coating to five types of different membrane substrate including mixed cellulose ester (MCE), PES, glass fiber, PVDF, and PTFE, respectively. This is the first ever presentation of an MCE membrane with a nano-pyramid surface structure. Our MCE also provided a superhydrophilic surface with underwater oleophobicity and the ability to tune the surface pore size. In the separation of O/W emulsions, our hybrid metal-organic membrane achieved the highest ever permeation flux of 1555 L m^{-2} h^{-1} (LMH) with selectivity exceeding 99%.

RESULTS AND DISCUSSION

Characterizations of coated membranes

Figure 1 compares SEM images of the five coated membranes [MCE, PVDF, PTFE, glass fiber (GF), and PES] together with bare membranes. SS deposition resulted in a nano-pyramidal surface structure with reduced surface pore size. The sizes of surface pores on the coated samples were as follows: MCE (156.1 nm), PES (224 nm), PVDF (342 nm), GF (41 nm), and PTFE (419 nm) (see Supplementary Figs. 1 and 2 in the Supplementary Information). In addition, we can see in the images that SS pyramids did not only grow on the surface but also covers the fiber underneath very well. Right-most column of Fig. 1 also presents the high-magnification views of coated MCE and PVDF. It shows that on the surface nano-pyramidal structures appeared larger (80–100 nm) and below the surface they appeared smaller (~20 nm or less). This is presumably due to the limited exposure to the SS sputtering target during deposition, for sputtering is considered a line-of-sight technique. Figure 2 shows the cross-section of a SS-coated MCE membrane after being fractured in half. The SS coating process increased the diameter of the thin fibers from ~200 to ~650 nm. Based on the micrographs, we also determined that the SS-coating had covered membrane fibers as deep as ~2.6 µm from the membrane surface. The presence of SS coatings on and near membrane surfaces was also verified using EDS element mapping (see Supplementary Fig. 3). The blue arrows indicate voids resulting from the forcible removal of fibers during sample cleavage. Otherwise, we observed no sign of brittle fracture in the SS coating, suggesting that the coating possesses essential ductility to be applied on a flexible membrane substrate,

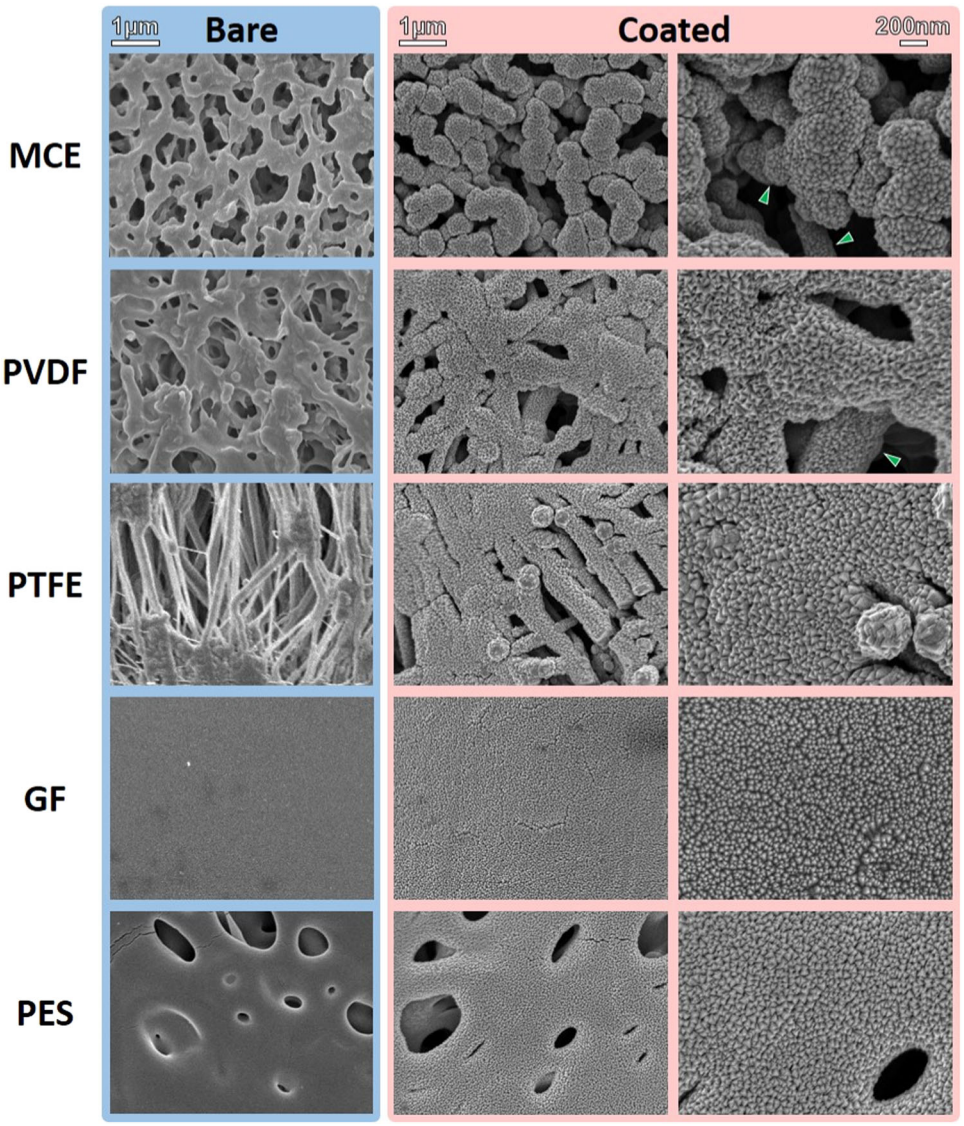

Fig. 1 Surface morphology of bare and coated membranes. Surface-view SEM micrographs showing bare and coated MCE, PVDF, PTFE, GF, and PES membranes. Green arrows in high-magnification views of coated MCE and PVDF indicate relatively small nano-pyramidal SS structures below the membrane surface.

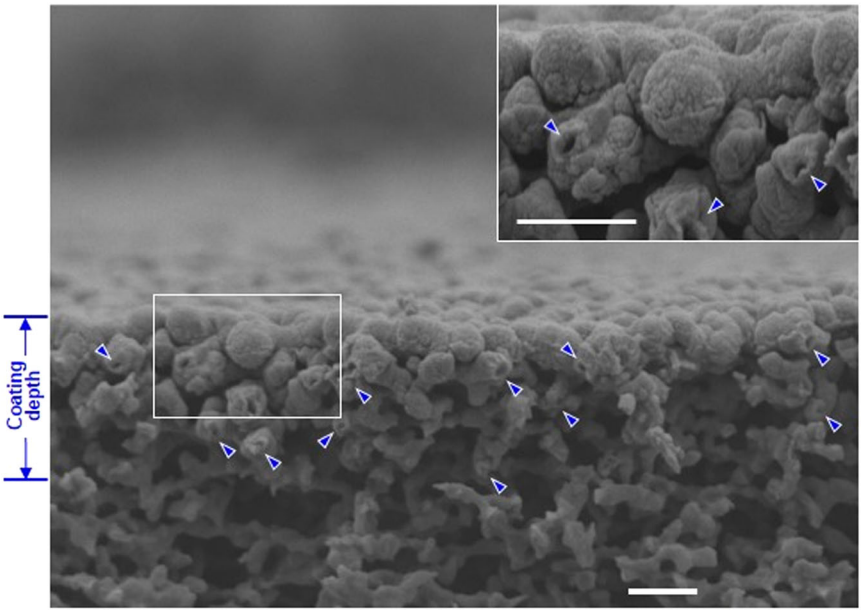

Fig. 2 Microstructure of a coated MCE membrane. Cross-sectional SEM micrographs of coated MCE membrane. Inset is a zoomed view of white-framed area. Blue arrows indicate voids resulting from the forcible removal of fibers during sample cleavage in liquid nitrogen. White scale bars indicate 1 μm.

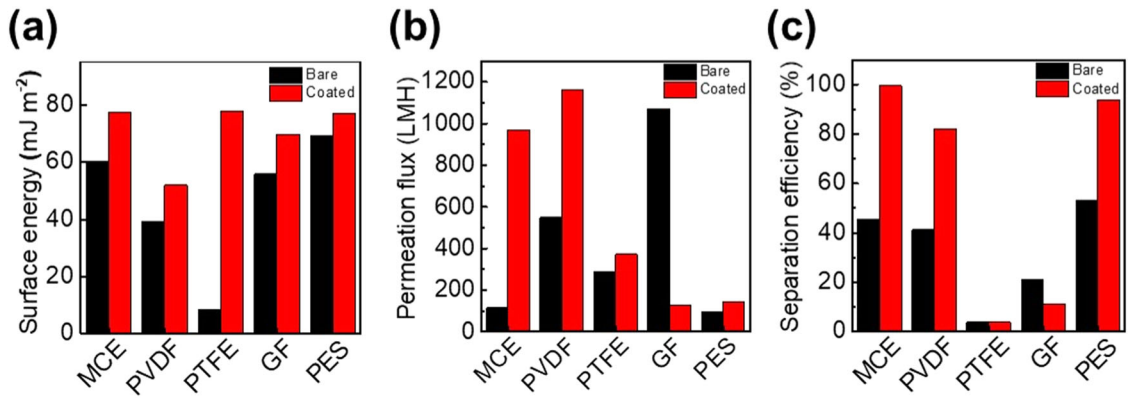

Fig. 3 Selected properties of bare and coated membranes. a Surface free energy; **b** permeation flux; **c** separation efficiency of five membranes in bare and coated states.

like MCE in this study. The ductility of the SS coating on coated membranes was assessed using ramp-loaded nano-scratch tests. Chemical, crystallographic, and microstructural analyses of SS coating have been performed using wavelength-dispersive X-ray spectroscopy, X-ray diffractometer, transmission electron microscopy, and grazing-incidence small-angle X-ray scattering. These results are presented in Supplementary Figs. 4 and 5.

We measured the surface energy of membranes before and after coating and the results are shown in Fig. 3a. All coated membrane samples, other than PVDF exhibited high surface energy (≥70 mJ m^{-2}). Moreover, SS coating had slightly increased the surface energy of all membranes. Except in PTFE its surface energy drastically increased from <10 to >75 mJ m^{-2} after coating. All coated membranes showed surface hydrophilicity (see Supplementary Fig. 6). To assess their separation performance, we prepared sodium dodecyl sulfate (SDS)–stabilized (SSE) O/W emulsions from hexadecane with drop diameters <6 μm as model emulsions. Resultant permeation flux and separation efficiency of bare and coated membranes are shown in Fig. 3b, c, respectively. The increase in permeation flux before and after SS coating was most pronounced in MCE (from ~108 to ~954 LMH), followed by PVDF (from ~522 to ~1,130 LMH), while negligible in PES and PTFE. In GF, the permeation flux was drastically reduced, probably due to a significant reduction in surface pore size (see Supplementary Fig. 1) during coating. Overall, coating MCE, PVDF, and PES samples with SS-nanopyramid can increase their separation efficiency by 119, 99, and 76%, respectively. After coating, the rough MCE substrate presented a coral-like hierarchical structure (nano and micron channels), which proved beneficial to oil/water separation performance. SS coating did not have a significant effect on the separation efficiency of PTFE or GF membranes.

Based on the above observations, we selected MCE for subsequent experiments optimizing the deposition parameters of SS nanopyramid. Results of which are shown in SEM images under various magnifications in Fig. 4. The samples were designated according to coating thickness on Si as follows: MCE A (1060 nm), MCE B (1680 nm), MCE C (475 nm), and MCE D (672 nm). The average surface pore sizes were as follows: MCE A (11.9 ± 2.7 nm), MCE B (72.6 ± 4.7 nm), MCE C (156.1 ± 6.8 nm), and MCE D (875.1 ± 12.5 nm) (see Supplementary Fig. 2). Overall, we observed a negative correlation between

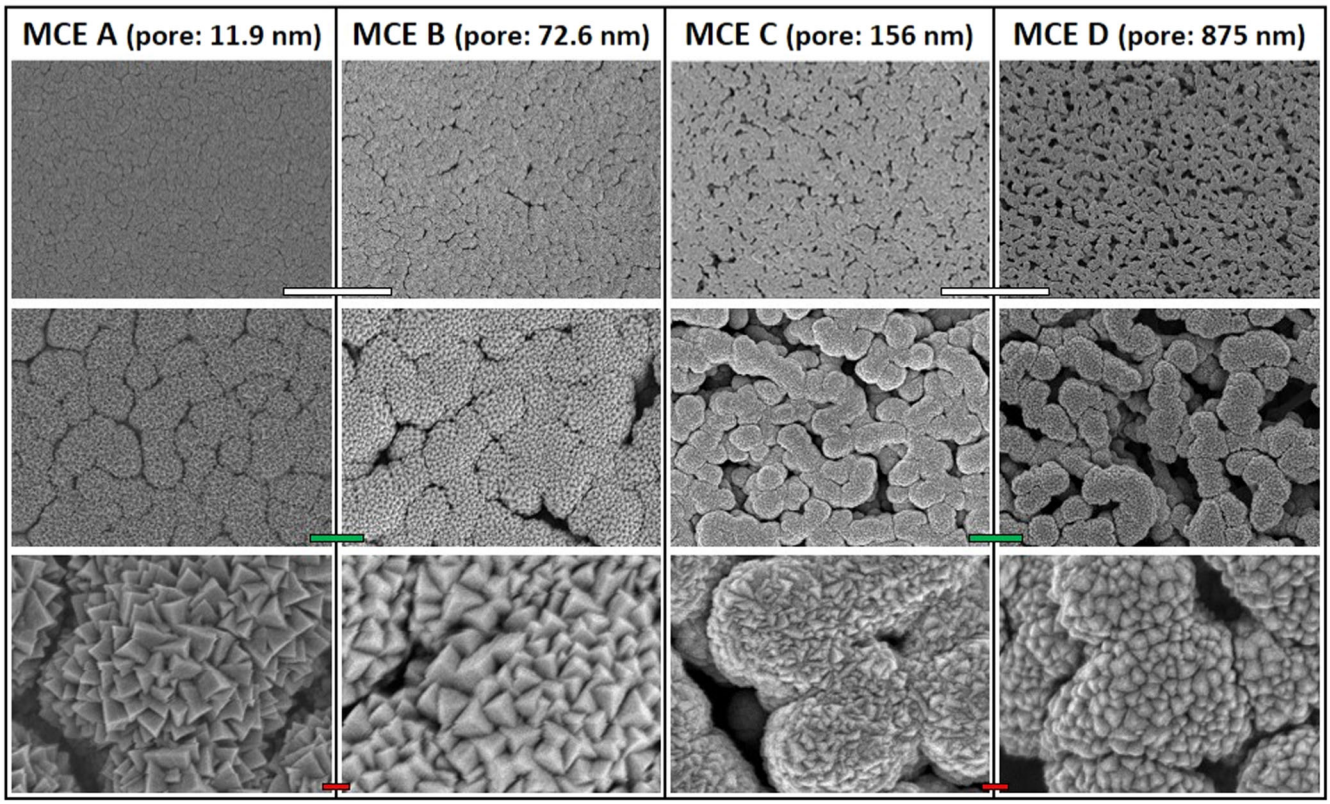

Fig. 4 Microstructure of coated MCE membranes. Surface-view SEM micrographs of four coated MCE membranes (MCE A, MCE B, MCE C, and MCE D) at various magnifications with their respective average surface pore sizes. White, green, and red scale bares represent 10 µm, 1 µm, and 100 nm, respectively.

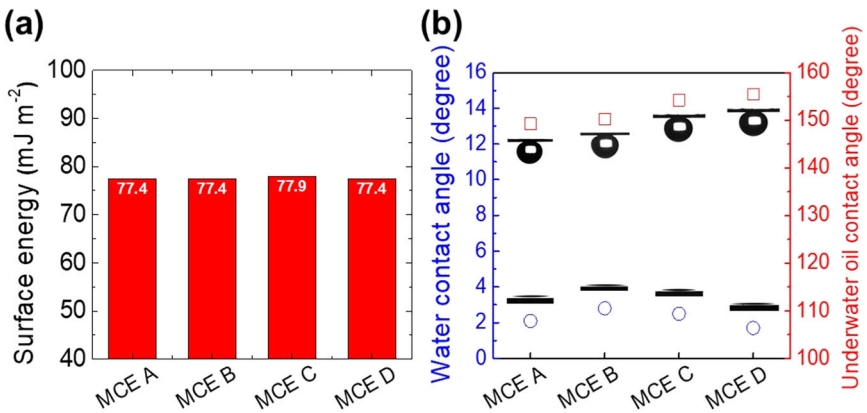

Fig. 5 Superhydrophilicity and superoleophobicity. a Surface free energy; **b** water contact angle in air (blue) and oil contact angle under water (red) of four coated MCE membranes.

coating thickness and surface pore size, due to the blockage of pores during deposition. All four coatings presented pyramidal nanostructures with following pyramid sizes: MCE A (~125–150 nm), MCE B (~70–120 nm), MCE C (~20–50 nm), and MCE D (~50–80 nm). Note that the pyramidal structure size increased with coating thickness. The size of the pyramidal structures was correlated with the thickness of the coatings, which in turn was correlated with the time allotted for grain growth and subsequent surface deposition.

Separation performance of surfactant-stabilized O/W emulsions

The mechanism underlying separation was elucidated by measuring the surface free energy of the coated MCE membranes using the Owens-Wendt method[25], and the results are summarized in Fig. 5a. Regardless of differences in the size of the pores or nanopyramids, all coated MCE membranes exhibited high surface free energy (>77 mJ m^{-2}), which is indicative of superhydrophilicity. This is proved in Fig. 5b that their water contact angle measurements obtained in air were <4°. We performed oil contact angle measurements using hexadecane with the samples submerged in water. All MCE membranes presented underwater superoleophobicity, with those of MCE C and MCE D exceeding 150°. Therefore Fig. 5 justifies that their high emulsion separation performance can be attributed to the possession of both superhydrophilicity and underwater superoleophobicity.

Based on the above research, MCE C was further subjected to separation test using light oils (hexane, mineral oil, xylene,

toluene, and hexadecane) with SDS surfactant. As shown in Fig. 6a, the resultant separation efficiency exceeded 99% for all oils and even reached 99.99% when applied to toluene and hexadecane. Details of oil droplet size distribution and optical micrographs of feed emulsions and filtrates are shown in Supplementary Fig. 7. Supplementary Figure 8 presents a plausible mechanism of the separation. The permeability of pure water and hexadecane-in-water emulsion using coated MCE membranes were characterized and the result is shown in Supplementary Fig. 9. Furthermore, the permeation flux was estimated to be 922–1035 LMH for mineral oil, hexane, xylene, and hexadecane emulsions, while 1555 LMH for toluene emulsion. As shown in Fig. 6b, the coated MCE C membrane exhibited satisfactory permeation flux over a wide range of viscosities and densities. We can see that viscosity is not a determining factor on permeation flux, as evidenced by the fact that the emulsion with mineral oil (the highest viscosity) was 922 LMH, which is comparable to that of the other emulsions. The high permeation flux for the toluene emulsion can be attributed to low density and low viscosity.

We prepared a number of emulsions to emulate the harsh conditions often encountered treating industrial oily wastewater in real-world situations, such as oil spills at sea. We prepared an anionic O/W emulsion (with the addition of SDS), an oil-in-acid emulsion (HCl, with a pH value of 1), and an oil-in-alkali emulsion (NaOH, with a pH value of 14), and an oil-in-sea water emulsion (3 g NaCl in 100 g water). Figure 7a presents the separation performance of MCE C when applied to these emulsions at 25 and 60 °C. MCE C exhibited excellent separation performance (>99% separation efficiency) with high permeation flux (>945 LMH), regardless of the emulsion conditions.

The anti-fouling performance and recyclability of the SS membranes were analyzed in four-cycle filtration experiments. Hexane-in-water emulsion was fed through the membrane under a constant pressure of 0.8 bar, the results of which (through 4 cycles) are shown in Fig. 7b. The initial water flux for the surfactant-stabilized toluene-in-water emulsion (1012 LMH) decreased slightly, eventually stabilizing after 4 cycles (970 LMH). This decrease in water flux can be attributed to an oil filter cake layer blocking the surface pores[26,27], despite the fact that between each cycle, the membranes were flushed using ethanol and deionized water to remove the filter cake, thereby recovering water flux to the initial level, such that oil rejection performance in the second, third, and fourth cycles remained at close to 99%. As shown in Supplementary Fig. 10, the coated MCE films presented excellent durability and flexibility, as evidenced by testing involving flexural strain of 0.66% for up to 2,000 cycles. Overall, the robust SS-coated membrane exhibited outstanding recyclability and anti-oil fouling capability, thereby making it ideal for long-term applications (see oxidation result in Supplementary Fig. 11 and adhesion test results in Supplementary Figs. 12–14).

The superhydrophilicity of the surface-modified membranes also enabled excellent underwater anti-oil adhesion capability, as evidenced by DCE droplet sliding off of the surface (see Fig. 8)[21]. Note that the bare MCE membrane presented complete adsorption of DCE. These results can be attributed to the nano-hierarchical structure of the SS coating and corresponding

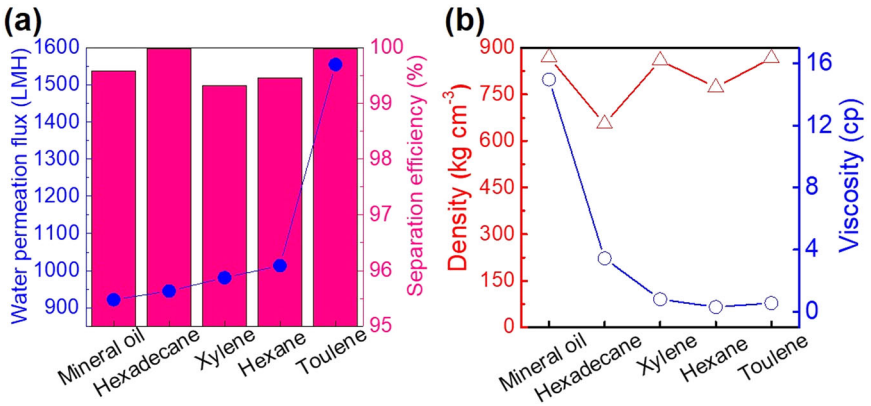

Fig. 6 Emulsion separation performance of coated membranes. a Water permeation flux and separation efficiency for various light oils-in-water emulsions for coated MCE C membrane; **b** density and viscosity for various surfactant-stabilized O/W emulsions.

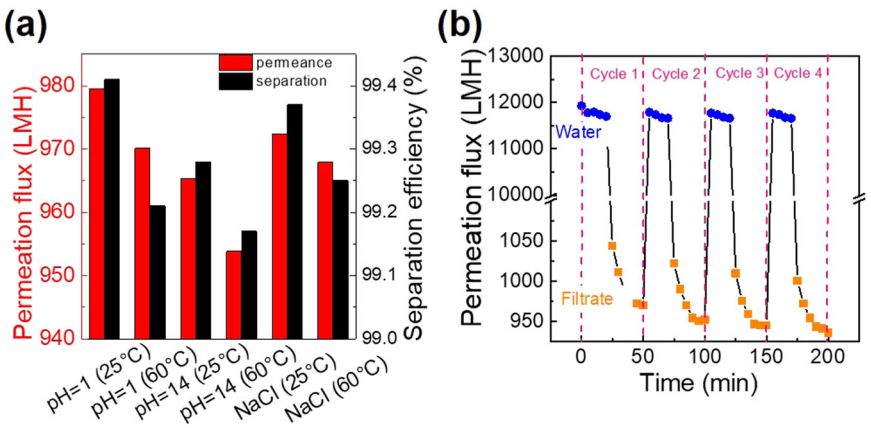

Fig. 7 Emulsion separation in harsh conditions and anti-fouling performance. a Permeation flux of MCE C when applied to the emulsion of hexadecane in water under harsh environments (pH = 1, pH = 14, and 3% NaCl); **b** separation performance and flux recovery of coated MCE C membrane.

Cassie-Baxter state at the interface, which allowed the trapping of water to form a thin hydration layer preventing the adhesion of oil droplets[28,29]. Our numerical simulation results in Supplementary Fig. 15 support our assertion that a zigzag channel wall (created by the pyramidal SS coating) enhanced resistance to the flow of oil particles. Note that the physical gaps in the zigzag configuration also created a three-dimensional structure, which was well-suited to the flow of water.

Comparison with other membranes

Figure 9 compares separation efficiency of the proposed MCE C membrane and previous membranes, including polymer-based, inorganic-based, composite, gel, and self-healing membranes when applied to O/W emulsions[30–71]. Note that MCE C outperformed by two-fold all existing membranes, while retaining high separation efficiency [Fig. 9a]. The size of MCE C (~156 nm) achieved the highest overall permeance (nearly 1600 LMH), exceeding by three-fold that of previous membranes [Fig. 9b]. The outstanding O/W separation performance can be attributed to the superhydrophilicity and underwater superoleophobicity provided by the nano-pyramidal SS coating. In summary, this study opens the door to the sputter deposition of stainless-steel coatings on polymers to enable the large-scale room-temperature fabrication of high-performance membranes for O/W emulsion separation.

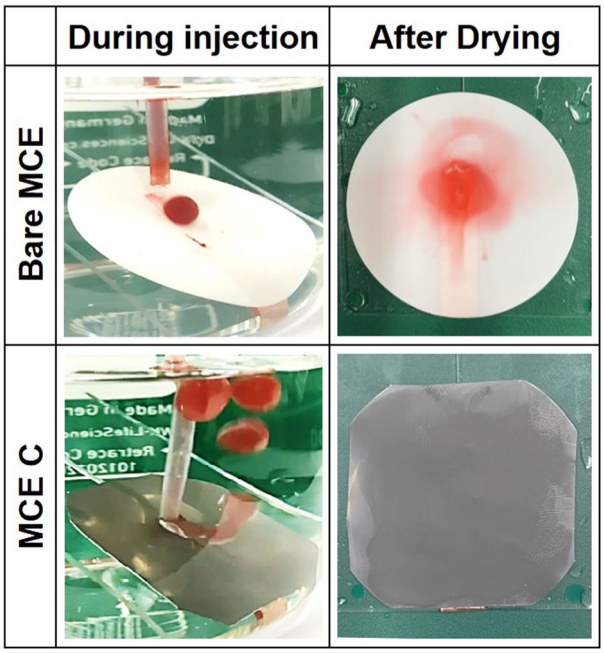

Fig. 8 Anti-oil adhesion capability. Photographs of bare MCE and coated MCE C during injection of toluene oil (dyed with Congo Red) and after drying.

This paper reports on a high-permeable and high-selective membrane for O/W emulsion separation, fabricated by sputtering a thin coating of stainless steel on a polymer substrate. The proposed SS coating presents a nano-pyramidal structure with superhydrophilicity, underwater superoleophilicity as well as outstanding antifouling capability. The SS coating on an MCE surface presented pyramidal nanostructures measuring ~20–50 nm in size and an average surface pore size of 156.1 nm. Separation performance was evaluated using five light oil-water emulsions with various viscosities and densities (mineral oil, xylene, toluene, hexane, and hexadecane). The coated membrane achieved separation efficiency of >99% when applied to light oil-water emulsions with a range of viscosities and densities, and the highest ever permeation flux of 1555 LMH when applied to toluene-in-water emulsions. The membrane also presented outstanding recyclability, as evidenced by oil rejection of >99% through four cycles. The coated membrane was shown to work well under harsh conditions, including salty water, extreme pH values (1–14), and high temperatures (60 °C). The membrane also presented high selectivity and permeation flux of not less than 945 LMH. The proposed SS coating deposited using a highly scalable and straightforward sputtering technique at room temperature could easily be scaled up for the mass production of high-performance membranes for O/W emulsion separation.

METHODS

The magnetron sputtering of stainless steel (SS) coatings was performed using a 3-inch sputtering target of commercial SUS316 SS under high purity argon with a base pressure of $<10^{-6}$ Torr and working pressure of 12 mTorr without intentional substrate heating. Further details of the nano-pyramid structure can be referred to our previous article[24]. Thin films of SS were deposited on a variety of substrates, including mixed cellulose ester membrane (MCE) filters (ADVANTEC, φ47 mm, pore size 0.2 μm), PES, glass fiber (GF), PVDF, and PTFE. The substrates (35 mm × 35 mm) were rotated during deposition to ensure uniform deposition. To facilitate thickness measurements and cross-

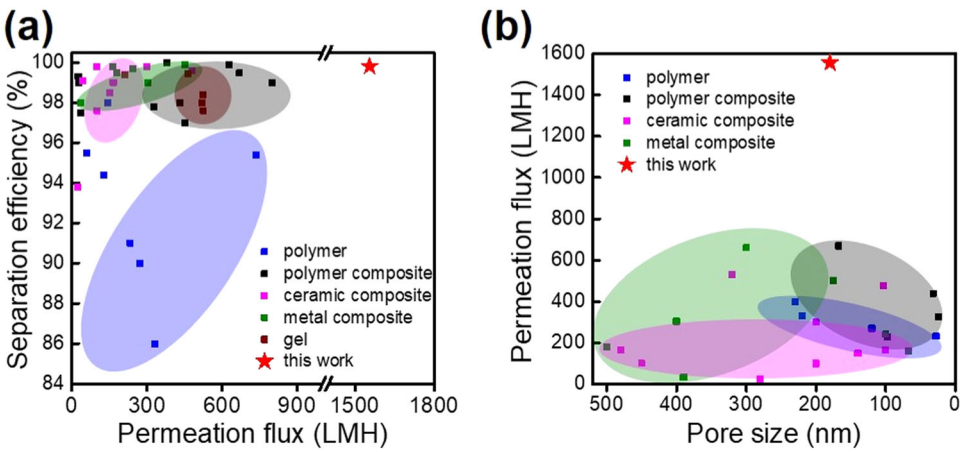

Fig. 9 Outperforming by two-fold all membranes. Performance comparison of **a** separation efficiency, permeation flux, and **b** pore size of our coated MCE C relative to other membranes developed for oil/water emulsion separation.

sectional observations, we had also deposited SS coatings on p-type (100) silicon wafers under the same deposition conditions.

Surfactant-stabilized O/W emulsions were prepared by mixing sodium dodecyl sulfate (SDS) with five types of oil (Hexadecane, mineral oil, n-hexane, toluene, and m-xylene) in deionized water at a volume ratio of 1:10:0.02 (oil: water: surfactant). The O/W mixture was subjected to ultrasonication treatment for 1 h followed by stirring overnight to create a well-mixed stable emulsion. Separation experiments were conducted under low vacuum pressure (0.8 bar) using a dead-end filtration cell with an effective separation area of 1.9×10^{-4} m^2. Note that the solution was stirred for at least 24 h prior to use. The SS-coated membrane was fixed between a filtration cell with the hydrophilic side (coated surface) facing upward.

Prior to each separation cycle, the membrane was pre-wetted with DI water to form a hydration layer. After pouring the emulsion into a feed funnel, the permeate was collected and analyzed in terms of oil content in a dead-end system. Permeation flux (J) and separation efficiency (R) were estimated using the following equations[8,72]:

$$J\left(L \cdot m^{-2} \cdot h^{-1}\right) = \frac{V}{A \cdot \Delta t} \quad (1)$$

where V indicates the permeate volume (L), A is the effective membrane area (m^2), and Δt indicates the permeation time (h).

$$R(\%) = \left(1 - \frac{C_f}{C_o}\right) \times 100\% \quad (2)$$

where R indicates the separation efficiency, and C_f and C_o respectively indicate the concentrations of oil in the permeate and emulsion feed. Oil content was analyzed using a wastewater treatment photometer (HI 83214, HANNA Inst.), in which the chemical oxygen demand (COD) was measured. The chemical stability of the SS-coated membranes were evaluated over a period of 2 h under various harsh environmental conditions, including high acidity (HCl, pH = 1), alkalinity (NaOH, pH = 14), and saltiness (3 g NaCl in 100 g water) at 60 °C[73]. Chemical stability was evaluated by measuring the water contact angle of the SS-coated surface before and after immersion.

Surface wettability and surface energy were measured using a contact angle goniometer [Phoenix-MT(A)]. An optical microscope (Axioskop, Zeiss) was used to observe the characteristics of O/W emulsions, a rheometer (DV-III programmable rheometer, Brookfield) was used to measure viscosity, and dynamic light scattering (Zeta Nanosizer, 177 Malvern) was used to determine oil droplet sizes. The self-cleaning performance of the membrane surface was evaluated by applying droplets of 1,2-dichloroethane (DCE) oil dyed with Congo Red and then immersing the membrane in water. Note that the DCE oil droplets rolled off the surface without leaving any trace.

The surface morphology of SS coating and membranes were observed using a field-emission scanning electron microscope (SEM, JEOL 7900F) and an X-ray energy dispersive spectroscope (EDS, Oxford Ultim Max 100). SEM was also used to analyze the surface pore-size distribution[33]. The compositions of SS coatings and bare MCE membranes were characterized using an X-ray wavelength dispersive spectroscope (WDS) with an electron probe micro-analyzer (EPMA, JEOL JXA-8530F Plus). Cross-sectional SEM images of the coated membranes were obtained after fracturing samples in a liquid nitrogen bath, in order to preserve their as-coated appearance as much as possible. The crystallographic structure of the SS coating itself was measured using an X-ray diffractometer (Bruker, D8 DISCOVER SSS Multi-Function High Power X-Ray Diffractometer) with Cu Kα radiation at 40 KV and 100 mA. The operating parameters of XRD measurement included a glancing angle of 0.5° and scanning area (2θ) ranging from 20° to 100° in 0.05° increments with a step time of 0.5 s. Transmission electron microscopy (TEM) was performed using a high-resolution Philips Tecnai F20 G2 system operated at 200 kV. Cross-sectional TEM samples were prepared via dual-beam focused ion beam (FIB) milling using an FEI Quanta 3D FEG. Samples were then lifted out using a glass manipulator needle and placed on a carbon-coated Cu grid (Ted Pella, Inc., 300 mesh) for TEM observation. Note that prior to FIB milling, Pt was deposited on the coatings as a protective layer to minimize ion damage during milling.

The anti-fouling performance (recyclability) of the SS-coated MCE membranes was assessed in a four-cycle filtration experiment involving a toluene-in-water emulsion flowing across the membrane. Flux recovery was determined by recording the permeation flux every 2 min over a period of 20 min. Between cycles, the membrane surfaces were flushed with ethanol, followed by a deionized water rinse for 20 mins to remove residual oil. Moreover, the mechanical durability of SS-coated MCE was assessed by bending tests up to a bending radius of ~3 mm. A total of 2000 bending cycles were conducted at 3 Hz. We evaluated the O/W emulsion separation efficiency and sheet resistance of the coated membranes at intervals of 500 bending cycles. Then sheet resistance was measured using four-point probe method, with the aim of elucidating the effects of bending to the structural stability of the SS coating and its adhesion to the membrane.

DATA AVAILABILITY

The data associated with the manuscript are included with Supplementary Information and available on reasonable request.

Received: 23 October 2022; Accepted: 13 February 2023;
Published online: 03 March 2023

REFERENCES

1. Blumer, M. *Oil on the Sea* (ed. Hoult, D. P.) (Springer, 1969).
2. Klekowski, E. J. Jr, Corredor, J. E., Morell, J. M. & Del Castillo, C. A. Petroleum pollution and mutation in mangroves. *Mar. Pollut. Bull.* **28**, 166–169 (1994).
3. Aoudj, S., Khelifa, A., Drouiche, N. & Hecini, M. Removal of fluoride and turbidity from semiconductor industry wastewater by combined coagulation and electroflotation. *Desalin. Water Treat.* **57**, 18398–18405 (2016).
4. Jernelöv, A. How to defend against future oil spills. *Nature* **466**, 182–183 (2010).
5. Blumer, M. & Sass, J. Oil pollution: persistence and degradation of spilled fuel oil. *Science* **176**, 1120–1122 (1972).
6. Xue, Z., Cao, Y., Liu, N., Feng, L. & Jiang, L. Special wettable materials for oil/water separation. *J. Mater. Chem. A* **2**, 2445–2460 (2014).
7. Wang, B., Liang, W., Guo, Z. & Liu, W. Biomimetic super-lyophobic and super-lyophilic materials applied for oil/water separation: a new strategy beyond nature. *Chem. Soc. Rev.* **44**, 336–361 (2015).
8. Kota, A. K., Kwon, G., Choi, W., Mabry, J. M. & Tuteja, A. Hygro-responsive membranes for effective oil–water separation. *Nat. Commun.* **3**, 1–8 (2012).
9. Bank, W. *Pollution Prevention and Abatement Handbook, 1998: Toward cleaner production*. (The World Bank, 1999).
10. Reynolds, J. G., Coronado, P. R. & Hrubesh, L. W. Hydrophobic aerogels for oil-spill clean up–synthesis and characterization. *J. Non-Cryst. Solids* **292**, 127–137 (2001).
11. Chen, N. & Pan, Q. Versatile fabrication of ultralight magnetic foams and application for oil–water separation. *ACS Nano* **7**, 6875–6883 (2013).
12. Calcagnile, P. et al. Magnetically driven floating foams for the removal of oil contaminants from water. *ACS Nano* **6**, 5413–5419 (2012).
13. Howarter, J. A., Genson, K. L. & Youngblood, J. P. Wetting behavior of oleophobic polymer coatings synthesized from fluorosurfactant-macromers. *J. Membr. Sci.* **3**, 2022–2030 (2011).
14. Kota, A. K. & Tuteja, A. High-efficiency, ultrafast separation of emulsified oil–water mixtures. *NPG Asia Mater.* **5**, e58–e58 (2013).
15. Wu, B. Membrane-based technology in greywater reclamation: a review. *Sci. Total Environ.* **656**, 184–200 (2019).
16. Tseng, H.-H., Wu, J.-C., Lin, Y.-C. & Zhuang, G.-L. Superoleophilic and superhydrophobic carbon membranes for high quantity and quality separation of trace water-in-oil emulsions. *J. Membr. Sci.* **559**, 148–158 (2018).
17. Huang, A. et al. Fabrication of zinc oxide nanostructure coated membranes for efficient oil/water separation. *J. Membr. Sci.* **566**, 249–257 (2018).

18. Huang, A. et al. Nanoarchitectured design of porous ZnO@ copper membranes enabled by atomic-layer-deposition for oil/water separation. *J. Membr. Sci.* **582**, 120–131 (2019).
19. Zhou, K. et al. Ultrathin cellulose nanosheet membranes for superfast separation of oil-in-water nanoemulsions. *Nanoscale* **6**, 10363–10369 (2014).
20. Park, H. B., Kamcev, J., Robeson, L. M., Elimelech, M. & Freeman, B. D. Maximizing the right stuff: The trade-off between membrane permeability and selectivity. *Science* **356**, eaab0530 (2017).
21. Ye, Q. et al. Metal-organic framework modified hydrophilic polyvinylidene fluoride porous membrane for efficient degerming selective oil/water emulsion separation. *npj Clean. Water* **5**, 23 (2022).
22. Chisca, S. et al. Polytriazole membranes with ultrathin tunable selective layer for crude oil fractionation. *Science* **376**, 1105–1110 (2022).
23. Chen, Y. et al. Fabrication of silica nanospheres coated membranes: towards the effective separation of oil-in-water emulsion in extremely acidic and concentrated salty environments. *Sci. Rep.* **6**, 32540 (2016).
24. Yiu, P., You, J.-D., Wang, S.-T. & Chu, J. P. Tunable hydrophilicity in a surface nanotextured stainless steel thin film deposited by DC magnetron sputtering. *Appl. Surf. Sci.* **555**, 149705 (2021).
25. Owens, D. K. & Wendt, R. Estimation of the surface free energy of polymers. *J. Appl. Polym. Sci.* **13**, 1741–1747 (1969).
26. Noamani, S., Niroomand, S., Rastgar, M. & Sadrzadeh, M. Carbon-based polymer nanocomposite membranes for oily wastewater treatment. *npj Clean. Water* **2**, 20 (2019).
27. Zhang, J. et al. Self-polishing emulsion platforms: eco-friendly surface engineering of coatings toward water borne marine antifouling. *Prog. Org. Coat.* **149**, 105945 (2020).
28. Lin, Y. et al. Development of Janus membrane with controllable asymmetric wettability for highly-efficient oil/water emulsions separation. *J. Membr. Sci.* **606**, 118141 (2020).
29. Gupta, P. & Kandasubramanian, B. Directional fluid gating by janus membranes with heterogeneous wetting properties for selective oil–water separation. *J. Membr. Sci.* **9**, 19102–19113 (2017).
30. Wang, D.-M. et al. A novel method for controlling the surface morphology of polymeric membranes. *J. Membr. Sci.* **169**, 39–51 (2000).
31. Xiong, Z. et al. Simple amphoteric charge strategy to reinforce superhydrophilic polyvinylidene fluoride membrane for highly efficient separation of various surfactant-stabilized oil-in-water emulsions. *J. Membr. Sci.* **12**, 47018–47028 (2020).
32. Khodadousti, S., Zokaee Ashtiani, F., Karimi, M. & Fouladitajar, A. Preparation and characterization of novel PES-(SiO_2-g-PMAA) membranes with antifouling and hydrophilic properties for separation of oil-in-water emulsions. *Polym. Adv. Technol.* **30**, 2221–2232 (2019).
33. Asad, A., Rastgar, M., Sameoto, D. & Sadrzadeh, M. Gravity assisted super high flux microfiltration polyamide-imide membranes for oil/water emulsion separation. *J. Membr. Sci.* **621**, 119019 (2021).
34. Deng, Y. et al. Fabrication of superhydrophilic and underwater superoleophobic membranes via an in situ crosslinking blend strategy for highly efficient oil/water emulsion separation. *J. Membr. Sci.* **569**, 60–70 (2019).
35. Deng, W., Fan, T. & Li, Y. In situ biomineralization-constructed superhydrophilic and underwater superoleophobic PVDF-TiO_2 membranes for superior antifouling separation of oil-in-water emulsions. *J. Membr. Sci.* **622**, 119030 (2021).
36. Cui, J. et al. Facile preparation of grass-like structured NiCo-LDH/PVDF composite membrane for efficient oil–water emulsion separation. *J. Membr. Sci.* **573**, 226–233 (2019).
37. Zhang, N. et al. Facile hydrophilic modification of PVDF membrane with Ag/EGCG decorated micro/nanostructural surface for efficient oil-in-water emulsion separation. *Chem. Eng. J.* **402**, 126200 (2020).
38. Gao, J., Wang, J., Xu, Q., Wu, S. & Chen, Y. Regenerated cellulose strongly adhered by a supramolecular adhesive onto the PVDF membrane for a highly efficient oil/water separation. *Green. Chem.* **23**, 5633–5646 (2021).
39. Gu, Y. et al. Poly (vinyl alcohol) modification of poly (vinylidene fluoride) microfiltration membranes for oil/water emulsion separation via an unconventional radiation method. *J. Membr. Sci.* **619**, 118792 (2021).
40. Faraji, M., Nabavi, S. R. & Salimi-Kenari, H. Fabrication of a PAN–PA6/PANI membrane using dual spinneret electrospinning followed by in situ polymerization for separation of oil-in-water emulsions. *N. J. Chem.* **44**, 13488–13500 (2020).
41. Chen, X. et al. Modified-MOF-808-loaded polyacrylonitrile membrane for highly efficient, simultaneous emulsion separation and heavy metal ion removal. *J. Membr. Sci.* **12**, 39227–39235 (2020).
42. Chen, M., Zhu, L., Dong, Y., Li, L. & Liu, J. Waste-to-resource strategy to fabricate highly porous whisker-structured mullite ceramic membrane for simulated oil-in-water emulsion wastewater treatment. *ACS Sustain. Chem. Eng.* **4**, 2098–2106 (2016).
43. Rashad, M., Logesh, G., Sabu, U. & Balasubramanian, M. A novel monolithic mullite microfiltration membrane for oil-in-water emulsion separation. *J. Membr. Sci.* **620**, 118857 (2021).
44. Zhang, D. et al. Superhydrophilicity and underwater superoleophobicity TiO_2/Al_2O_3 composite membrane with ultra low oil adhesion for highly efficient oil-in-water emulsions separation. *Appl. Surf. Sci.* **458**, 157–165 (2018).
45. Liu, R., Raman, A. K. Y., Shaik, I., Aichele, C. & Kim, S.-J. Inorganic microfiltration membranes incorporated with hydrophilic silica nanoparticles for oil-in-water emulsion separation. *J. Water Process. Eng.* **26**, 124–130 (2018).
46. Yang, Y. et al. Fabrication of palygorskite coated membrane for multifunctional oil-in-water emulsions separation. *Appl. Clay Sci.* **182**, 105295 (2019).
47. He, S. et al. Chemically stable two-dimensional MXene@ UIO-66-$(COOH)_2$ composite lamellar membrane for multi-component pollutant-oil-water emulsion separation. *Compos., Part B* **197**, 108188 (2020).
48. Qian, D. et al. Multilayer network membranes based on evenly dispersed nanofibers/Co_3O_4 nanoneedles for high-efficiency separation of micrometer-scale oil/water emulsions. *Adv. Mater. Interfaces* **5**, 1801004 (2018).
49. Vadodariya, N. & Meena, R. Protein-functionalized aerogel membranes for gravity-driven separation. *ACS Sustain. Chem. Eng.* **7**, 4814–4820 (2019).
50. Li, F., Bhushan, B., Pan, Y. & Zhao, X. Bioinspired superoleophobic/superhydrophilic functionalized cotton for efficient separation of immiscible oil-water mixtures and oil-water emulsions. *J. Colloid Interface Sci.* **548**, 123–130 (2019).
51. Yang, S. et al. Facile and sustainable fabrication of high-performance cellulose sponge from cotton for oil-in-water emulsion separation. *J. Hazard. Mater.* **408**, 124408 (2021).
52. Kim, S., Kim, K., Jun, G. & Hwang, W. Wood-nanotechnology-based membrane for the efficient purification of oil-in-water emulsions. *ACS Nano* **14**, 17233–17240 (2020).
53. Feng, L. et al. Preparation of a rice straw-based green separation layer for efficient and persistent oil-in-water emulsion separation. *J. Hazard. Mater.* **415**, 125594 (2021).
54. Chen, Q. et al. A novel photocatalytic membrane decorated with RGO-Ag-TiO_2 for dye degradation and oil–water emulsion separation. *J. Chem. Technol. Biotechnol.* **93**, 761–775 (2018).
55. Qian, D. et al. TiO_2/sulfonated graphene oxide/Ag nanoparticle membrane: in situ separation and photodegradation of oil/water emulsions. *J. Membr. Sci.* **554**, 16–25 (2018).
56. Yu, Z., Zeng, H., Min, X. & Zhu, X. High-performance composite photocatalytic membrane based on titanium dioxide nanowire/graphene oxide for water treatment. *J. Appl. Polym. Sci.* **137**, 48488 (2020).
57. Ezazi, M. et al. Selective Wettability membrane for continuous oil−water separation and in situ visible light-driven photocatalytic purification of water. *Glob. Chall.* **4**, 2000009 (2020).
58. Liu, W. et al. Efficient separation of crude oil-in-water emulsion based on a robust underwater superoleophobic titanium dioxide-coated mesh. *N. J. Chem.* **44**, 2705–2713 (2020).
59. Chen, X. et al. Durable and stable $MnMoO_4$-coated copper mesh for highly efficient oil-in-water emulsion separation and photodegradation of organic contaminants. *J. Membr. Sci.* **11**, 23789–23797 (2019).
60. Zhan, B. et al. Fabrication of superwetting Cu@ Cu_2O cubic film for oil/water emulsion separation and photocatalytic degradation. *Appl. Surf. Sci.* **496**, 143580 (2019).
61. Li, F. et al. A Mussel-inspired method to fabricate reduced graphene oxide/g-C_3N_4 composites membranes for catalytic decomposition and oil-in-water emulsion separation. *Chem. Eng. J.* **322**, 33–45 (2017).
62. Yu, Z. et al. A mussel-inspired method to fabricate a novel reduced graphene oxide/$Bi_{12}O_{17}Cl_2$ composites membrane for catalytic degradation and oil/water separation. *Polym. Adv. Technol.* **30**, 101–109 (2019).
63. Ye, H. et al. Robust and durable self-healing superhydrophobic polymer-coated MWCNT film for highly efficient emulsion separation. *Environ. Sci.: Nano* **6**, 1259–1266 (2019).
64. Li, Y. et al. Robust graphene/poly (vinyl alcohol) janus aerogels with a hierarchical architecture for highly efficient switchable separation of oil/water emulsions. *J. Membr. Sci.* **11**, 36638–36648 (2019).
65. Li, X. et al. Asymmetric superwetting configuration of Janus membranes based on thiol–ene clickable silane nanospheres enabling on-demand and energy-efficient oil–water remediation. *J. Mater. Chem. A* **7**, 10047–10057 (2019).
66. Yang, C. et al. Design of a Janus F-TiO_2@ PPS porous membrane with asymmetric wettability for switchable oil/water separation. *J. Membr. Sci.* **11**, 22408–22418 (2019).
67. Chang, Q., Zhou, J.-e, Wang, Y., Wang, J. & Meng, G. Hydrophilic modification of Al_2O_3 microfiltration membrane with nano-sized γ-Al_2O_3 coating. *Desalination* **262**, 110–114 (2010).

68. Zou, D., Qiu, M., Chen, X., Drioli, E. & Fan, Y. One step co-sintering process for low-cost fly ash based ceramic microfiltration membrane in oil-in-water emulsion treatment. *Sep. Purif. Technol.* **210**, 511–520 (2019).
69. Chang, Q. et al. Application of ceramic microfiltration membrane modified by nano-TiO_2 coating in separation of a stable oil-in-water emulsion. *J. Membr. Sci.* **456**, 128–133 (2014).
70. Yang, C., Zhang, G., Xu, N. & Shi, J. Preparation and application in oil–water separation of ZrO_2/α-Al_2O_3 MF membrane. *J. Membr. Sci.* **142**, 235–243 (1998).
71. Abbasi, M., Mirfendereski, M., Nikbakht, M., Golshenas, M. & Mohammadi, T. Performance study of mullite and mullite–alumina ceramic MF membranes for oily wastewaters treatment. *Desalination* **259**, 169–178 (2010).
72. Zhu, P., Kong, T., Tang, X. & Wang, L. Well-defined porous membranes for robust omniphobic surfaces via microfluidic emulsion templating. *Nat. Commun.* **8**, 15823 (2017).
73. He, M. et al. Non-organic solvent prepared nanofiltration composite membrane from natural product tannic acid (TA) and cyclohexane-1, 4-diamine (CHD). *Sep. Purif. Technol.* **223**, 250–259 (2019).

ACKNOWLEDGEMENTS

This work is supported by National Science and Technology Coucil (Taiwan) (NSTC 111–2221-E-011-118, 111-2622-E-011-022, 111-2634-F-002-016, and 111-2221-E-002-015-MY3) and Ministry of Education (Taiwan) Higher Education Sprout under the Feature Area Research Center Program (111L9006).

AUTHOR CONTRIBUTIONS

J.P.C. and K.L.T. designed the experiments and developed the theory. Y.J.Y., J.D.Y., T.H.C., and J.R.L. performed the experiment including membrane coating, characterization, and performance tests. Y.L.S. performed simulation. Y.J.Y., J.P.C., P.Y., and K.L.T. prepared original draft, review & editing, and completed the manuscript. W.H.C., P.Y., and C.H.H. provided methodology and resources. All coauthors discussed the results and reviewed the manuscript.

COMPETING INTERESTS

The authors declare no competing interests.

ADDITIONAL INFORMATION

Supplementary information The online version contains supplementary material available at https://doi.org/10.1038/s41545-023-00237-x.

Correspondence and requests for materials should be addressed to Jinn P. Chu or Kuo-Lun Tung.

Reprints and permission information is available at http://www.nature.com/reprints

Publisher's note Springer Nature remains neutral with regard to jurisdictional claims in published maps and institutional affiliations.